

Time-resolved observation of a dynamical phase transition with atoms in a cavityT. W. Clark,¹ A. Dombi,¹ F. I. B. Williams,¹ Á. Kurkó,^{1,2} J. Fortágh,³ D. Nagy,¹ A. Vukics,¹ and P. Domokos¹¹*Institute for Solid State Physics and Optics, Wigner Research Centre for Physics, P.O. Box 49, H-1525 Budapest, Hungary*²*Department of Physics of Complex Systems, Eötvös Loránd University, H-1117 Budapest, Hungary*³*Physikalisches Institut, Eberhard Karls Universität Tübingen, Auf der Morgenstelle 14, D-72076 Tübingen, Germany*

(Received 8 June 2021; revised 21 January 2022; accepted 1 June 2022; published 17 June 2022)

We present a dynamical, multilevel atom-cavity blockade effect and monitor its breakdown transition in time. As in the case of optical bistability, atoms initially impede transmission by detuning a cavity mode from the driving laser. The interacting system, however, eventually transitions into an uncoupled state via a critical runaway process, resulting in maximum transmission. These two extremes of transmission are macroscopic reflections of well-defined atomic states, and thus are interpreted as phases of a dynamical transition. By monitoring the output of the cavity, we make time-resolved measurements of the order parameter and that of the enhanced photon number fluctuations. Considering these results for different cavity driving intensities, we establish finite-size scaling relations that suggest such a runaway effect is in fact a genuine dynamical phase transition.

DOI: [10.1103/PhysRevA.105.063712](https://doi.org/10.1103/PhysRevA.105.063712)**I. INTRODUCTION**

Cavity QED, with strong coupling between atoms and a single mode of a resonator, opened a way to study nonlinear light-matter interactions for different sizes of atomic media. A well-known example is that of *optical bistability* [1,2], where the output of an optical resonator filled with atoms can have two stable stationary solutions for the same input intensity, according to hysteresis. In the limit of low or high drive intensity, however, the cavity fully blockades or permits the transmission, respectively. Therefore, taking the drive intensity as the control parameter and the cavity transmission as the order parameter, this driven-dissipative open system exhibits a genuine phase transition. Hereafter we will consider the concept of dynamical phase transitions in relation to the nonanalytic change of the steady state at a critical point or domain of control parameters.

In practice, however, this general phenomenon has many different realizations depending on the specific nonlinear interaction in the cavity. The active medium can consist of two [3,4] or many-level atoms [5,6], or the origin of the nonlinearity can arise even from the collective motion of an atomic cloud [7–10]. A key parameter describing the nonlinearity is the cooperativity, $\mathcal{C} = Ng^2/\gamma\kappa$, where N is the number of atoms, g is the coupling strength between the resonator mode and a single atom (in terms of the single-photon Rabi frequency), and κ and γ are the linewidths of the mode and atomic resonance, respectively.

The cooperativity can then be used to define some of the regimes of interaction. Early experiments on many-atom systems showed optical bistability to occur for cooperativity $\mathcal{C} \gtrsim 1$: Where atoms were weakly coupled to a single, resolved cavity mode ($g \ll \kappa, \gamma$). For low drive, the atoms remain close to their ground states and the transmission is suppressed by their absorptive [11] or dispersive effects [12,13] on the mode. For high drive, the other robust state of bistability, the atoms are in a full statistical mixture of ground and excited states

due to saturation, averaging out any effect on the transmission of the laser through the resonator. In this type of bistability, the thermodynamic limit corresponds to weak coupling and a large number of atoms, all while keeping the cooperativity, $\mathcal{C} \propto Ng^2$, constant. In strongly coupled systems ($g > \kappa, \gamma$), however, the effect can be studied with a low number of atoms [14,15], far away from the thermodynamic limit. Although remnants of bistability have been observed experimentally in the limit of small numbers of atoms [16], even individually [17,18], full bistability and hysteresis effects were obscured by quantum fluctuations [19,20].

Recently, however, in the regime of extreme nonlinearity, $\mathcal{C} \gg 1$, it was discovered [21,22] that bistability appears even for a single two-level atom. In this case, the thermodynamic limit corresponds to infinite cooperativity, $\mathcal{C} \rightarrow \infty$, with $N = 1$, as opposed to $\mathcal{C} \sim 1$ and $N \rightarrow \infty$ [23]. In this quantum limit of bistability, for strong coupling and low drive intensity, the transmission is blocked by the lack of near-resonant levels in the highly nonlinear Jaynes-Cummings spectrum [24,25]. Increasing the drive intensity, the blockade breaks down in favor of the other branch via high-order multiphoton excitation processes [21]. A distinctive feature of this *photon blockade breakdown phase transition*, with respect to optical bistability, is that the phases are represented by pure quantum states of the coupled system. These are stabilized, with macroscopic signatures, due to a continuous measurement of the transmitted intensity. As the required strong-coupling regime is only available with circuit QED systems [26,27], an analogous phase transition was observed with a single superconducting artificial atom, coupled to a microwave resonator [28]. The effect has incited significant interest [23,29–34].

In this paper, we introduce a third blockade effect whose breakdown, in contrast to that of optical bistability, undergoes a dynamical phase transition involving multilevel atoms. In the limit of both high cooperativity, $\mathcal{C} \gg 1$, and large atom number, we realize a strong collective coupling of atoms to

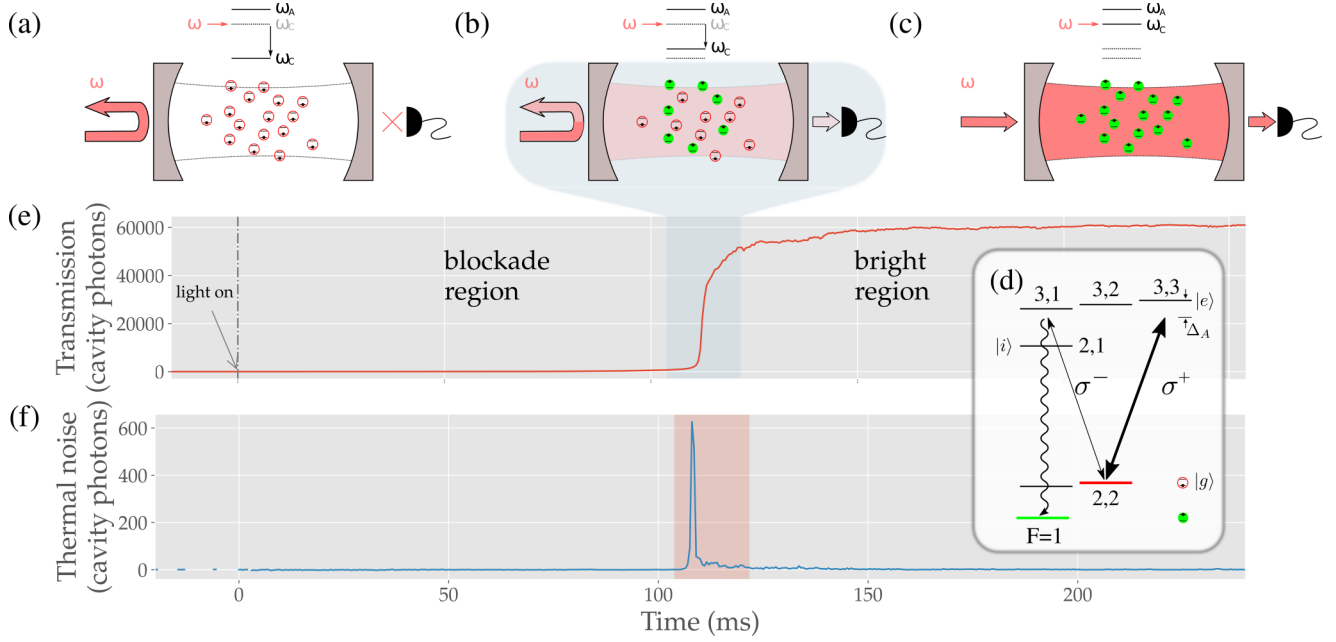


FIG. 1. Schematic representation of the transmission blockade breakdown phase transition. Atoms can be in (a) “red” (open circles) or (c) “green” (filled circles) states, blocking or permitting the light transmission through the cavity, respectively. (b) In the transition domain, the atoms are in a mixture of red (open) and green (filled) states. Upper level schemes show the cavity mode frequency with respect to the angular frequency of the pump laser, ω , and (d) red (open) and green (filled) states are identified with the hyperfine states of ^{87}Rb (only a part of the $5^2S_{3/2} \leftrightarrow 5^2P_{3/2}$ structure is shown). Far-off-resonance σ^- -polarized light provides an excitation path that assists the atoms’ escape from the blockading state, $|g\rangle$, to the $F = 1$ manifold of the electronic ground state. Atoms are first weakly excited to an intermediary state, $|i\rangle = (F, m_F) = (2, 1)$, before spontaneously decaying to the manifold, which is optically dark with respect to the cavity mode. (e) The time evolution of the transmitted intensity is plotted, exhibiting the switch from blockaded to transparent phase around 100 ms after turning on the cavity drive. It is expressed in units of cavity photon number deduced from the detected photon flux. (f) The transition is accompanied by the increase in cavity field fluctuations in terms of thermal photon numbers extracted from the displaced, thermal-state statistics of the transmitted light.

a mode of an optical cavity [35]. In our case, interaction between the cavity light field and the atomic transitions are dispersive, $\Delta_A \gg \gamma$, such that the relevant cooperativity parameter is $\mathcal{C}' = N g^2 / |\Delta_A| \kappa \approx 100$. Similarly to the photon blockade breakdown effect, there are two distinct, robust stationary states of the system, i.e., phases, in which the internal electronic state of the atoms is a pure quantum state. These are two atomic hyperfine ground states, associated with an empty and a highly excited coherent state of the cavity mode, respectively. The cavity photon number corresponds thus to an appropriate order parameter for the state of the system, which can be directly monitored in real time by measuring the photocurrent at the cavity output.

In the experiment, we study single transitions from one of the stationary states to the other. In particular, the system is prepared in an unstable phase and the transition to the stable phase is monitored, as if we observed the freezing of overcooled water. Since the large cooperativity brings the system close to the thermodynamic limit, the spontaneous collapse of the unstable phase takes place after a macroscopic waiting time. As the atoms were stably trapped in the resonator, we could not only observe these long periods in the unstable phase, but also obtain time-resolved recordings of the nonlinear runaway dynamics of the transition. The time resolution allows us, on the one hand, to see that the switchlike transition is not a measurement-induced quantum jump between atomic states, unlike the population shelving in fluorescence

measurements [36], and, on the other hand, to quantify the enhancement of photon number fluctuations found to accompany the transition. The amplitude of these fluctuations shows a power-law divergence with drive intensity to suggest a finite-size scaling approach to a phase transition [37–39].

II. TRANSMISSION BLOCKADE BREAKDOWN PHASE TRANSITION

The system and the basics of the transmission blockade phase transition are schematically represented in Fig. 1. A single, standing-wave mode of a cavity with frequency ω_C and linewidth κ is externally driven by coherent laser light at a frequency ω . The transmission of the laser through the cavity exhibits a Lorentzian resonance which is modified if atoms are present in the cavity. Consider a number of atoms, \mathcal{N} , with electric dipole resonance ω_A , which is far from the laser frequency, such that the atomic detuning, $\Delta_A = \omega - \omega_A$, satisfies $|\Delta_A| \gg \gamma$, where γ is the linewidth of the atomic resonance. In this limit, the atoms act on the light field as a dispersive medium. Each atom in its electronic ground state, $|g\rangle$, shifts the frequency of the mode by $\delta |f(\mathbf{r}_j)|^2$, where $\delta = g^2 / \Delta_A$, g is the single-photon Rabi frequency, $g = \sqrt{\frac{\omega_C}{2\epsilon_0 \hbar V}} d_{eg}$, and d_{eg} is the atomic dipole moment. The second factor of the shift is the spatial mode function for atom $j = 1, \dots, \mathcal{N}$. As the mode function, $f(\mathbf{r})$, is real and normalized to have a maximum of

1, the mode volume is $\mathcal{V} = \int d^3\mathbf{r} |f(\mathbf{r})|^2$. The frequency shift is additive and so the collective effect of the atoms gives a diminished transmission,

$$\frac{I_{\text{out}}}{I_0} = \frac{1}{(\Delta_C - N\delta)^2/\kappa^2 + 1}, \quad (1)$$

relative to the resonant transmitted intensity of the empty cavity, I_0 . For resonant drive, $\Delta_C = \omega - \omega_C = 0$, and a resonance shift much larger than the linewidth, $N\delta \gg \kappa$, the transmission is suppressed, which is the blockaded phase. The key variable governing the phase transition is the effective number of atoms, N , which depends both on the position and the internal state of the atoms:

$$N = \sum_{j=0}^{\mathcal{N}} |f(\mathbf{r}_j)|^2 p_j. \quad (2)$$

The internal state is represented by $p_j = \text{Tr}\{\hat{\rho}(|g\rangle\langle g| - |e\rangle\langle e|)\}$, the difference in probability for the j th atom to occupy the ground or excited state, respectively, where $|g\rangle \leftrightarrow |e\rangle$ labels the electric dipole transition coupled to the cavity mode. This concisely accounts for both a change in sign of the resonance, $-\delta$, due to population inversion and the actual number of atoms coupled to the mode, as optical pumping into dark states leads to $\text{Tr}\{\hat{\rho}(|g\rangle\langle g| + |e\rangle\langle e|)\} \neq 1$.

Initially, all of the atoms are prepared in the state $|g\rangle$, such that $p_j = 1$ for all j [Fig. 1(a)]. In the limit of cooperativity $C' \equiv N\delta/\kappa \rightarrow \infty$, the transmission would completely vanish, and the atoms, being in the dark, would remain in the ground state $|g\rangle$. Because of the finite C' , the blockaded phase is not stable; however, it protects itself for a long, macroscopic time. Some light infiltrating into the cavity leads to a small atomic excitation into $|e\rangle$, and an even smaller component into another state, $|i\rangle$ [cf. the level scheme in Fig. 1(d)]. From this latter state, the atoms can decay into a state decoupled from the cavity mode [green (filled) atoms in Fig. 1(b)]. Both of these processes, in turn, reduce the variable N and thus the collective mode shift, letting more light enter the cavity. This positive feedback loop is closed, causing a system runaway into the fully transparent state [Fig. 1(c)]. The occurrence of the transmission blockade breakdown after a significantly long time ($200 \text{ ms} \gg \gamma^{-1}, \kappa^{-1}$) and its associated dynamics are shown in Fig. 1(e).

III. EXPERIMENTAL REALIZATION AND MODELING

In our system, we used ^{87}Rb atoms: first captured from vapor in an ultrahigh-vacuum chamber and then precooled in a magneto-optical trap (MOT) above a high-finesse optical resonator. The atoms were further cooled by polarization gradient cooling to reach typical temperatures of $T \sim 100 \mu\text{K}$. Following an optical pumping cycle, the magnetically polarized sample of cold ^{87}Rb atoms in the $(F, m_F) = (2, 2)$ hyperfine ground state was loaded into a magnetic quadrupole trap. The magnetic trap center was shifted, in a controlled way, to transport the atoms vertically $\sim 1 \text{ cm}$ into the horizontally aligned cavity. The cavity is $l = 15 \text{ mm}$ long and so has a relatively large access from the direction transverse to the propagation axis. The mode waist, $w = 127 \mu\text{m}$, was an order of magnitude smaller than the size

of the atomic cloud in this direction, placing approximately $\mathcal{N} \sim 10^5$ atoms within the cavity mode volume. The mode linewidth was measured to be $\kappa = 2\pi \times 3.22 \text{ MHz}$ [half width at half maximum (HWHM)], and the single-atom coupling constant was calculated as $g = 2\pi \times 0.33 \text{ MHz}$ on the $(F, m_F) = (2, 2) \leftrightarrow (3, 3)$ hyperfine transition of the D2 line.

Such conditions were achieved by driving the fundamental Gaussian mode of the resonator with an appropriate laser through the incoupling mirror. The driving laser was locked to an atomic resonance and the resonator length was actively stabilized to the same atomic reference line via a transfer cavity at a far-detuned wavelength (805 nm). Thus the detuning, Δ_C , was an actively controlled variable, set on resonance, $\Delta_C = 0$, and far below the $F = 2 \leftrightarrow 3$ atomic resonance by $\Delta_A = -2\pi \times 35 \text{ MHz}$. The single-atom frequency shift was $\delta \approx 2\pi \times 3 \text{ kHz}$; thus an effective number of atoms, $N \approx 10^4$, led to a shift of the mode by more than 10κ away from resonance. The transmission was suppressed under these conditions.

The magnetic quadrupole trap was centered in the cavity mode; i.e., the mode was situated in the central plane of the trap where the magnetic field points radially outward from the symmetry axis. The atoms typically revolved around the (vertical) symmetry axis at a distance much larger than the mode waist. Within the cavity mode, therefore, the atoms experienced a magnetic field oriented parallel to the cavity axis. The quantization axis was thus aligned with the cavity axis, although pointing in opposite directions within each (longitudinal) half of the cavity mode. The circularly polarized light injected into the cavity, σ^+ , excited the $(F, m_F) = (2, 2) \leftrightarrow (3, 3)$ closed-cycle transition with a Clebsch-Gordan coefficient equal to 1 in one-half of the cavity. In the other half, however, the light effectively had a σ^- polarization with respect to the quantization axis and weakly drove the $(F, m_F) = (2, 2) \leftrightarrow (3, 1)$ transition and, off resonantly, the $(F, m_F) = (2, 2) \leftrightarrow (2, 1)$ transitions with Clebsch-Gordan coefficients of $1/15$ and $1/3$, respectively. This latter off-resonant excitation ($\Delta'_A = 230 \text{ MHz}$) by σ^- light led to optical pumping into the $F = 1$ manifold of the electronic ground state, which were dark states for the cavity field [cf. Fig. 1(d)]. As this two-photon transition involved a virtual excitation of the state $|i\rangle$, intracavity intensity was needed. This constituted a nonlinear decay channel for losing atoms from state $|g\rangle$, the state blockading the cavity transmission. Such an effect can underlie the phase-transition-like switch from the ensemble of atoms in the state $(F, m_F) = (2, 2)$ to the state $(F, m_F) = (1, m_F)$, with $m_F = 0, 1$. A simple semiclassical model captures the phase transition dynamics. The usual atom-cavity interaction is complemented by an additional loss process with rate Γ describing the escape to the dark states by spontaneous emission from the excited state. The mean-field approximation to the full quantum problem leads to the equations

$$\begin{aligned} \dot{a} &= (i\Delta_C - \kappa)a + gM + \eta, \\ \dot{M} &= (i\Delta_A - \gamma - \Gamma)M + g[N_e - N_g]a, \\ \dot{N}_e &= -g[a^*M + M^*a] - 2(\gamma + \Gamma)N_e, \\ \dot{N}_g &= g[a^*M + M^*a] + 2\gamma N_e, \end{aligned} \quad (3)$$

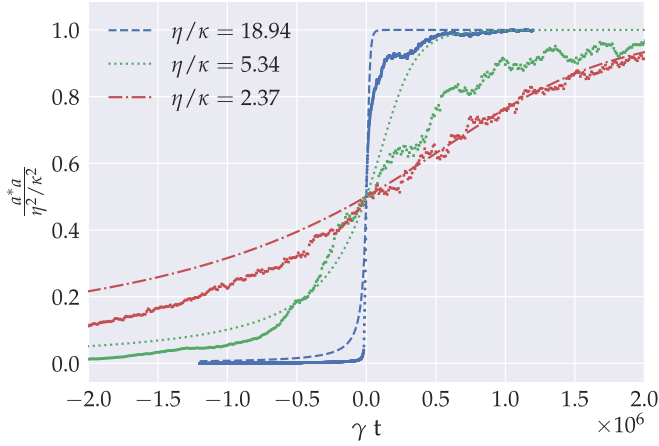


FIG. 2. The time evolution of the intracavity intensity around the phase transition for both the measurement data (squares) and the mean-field simulation (dashed, dotted, and dash-dotted lines). A selection of external laser drive powers, in units of the corresponding empty cavity photon number $(\eta/\kappa)^2$, are presented, where increasing drive power leads gradually from a crossover to the transmission blockade breakdown phase transition. After horizontally shifting the curves to have a common midpoint, the simplified model, with a single fitting parameter Γ , simultaneously accounts well for the slope of the transition for all drive powers ($\Gamma = 0.93 \times 10^{-3}\gamma$).

where a is the complex amplitude of the cavity field mode driven by the effective amplitude, η . Concerning the other variables, $M = \mathcal{N} \text{Tr}\{|g\rangle\langle e|\}$ describes the atomic polarization and $N_g = \mathcal{N} \text{Tr}\{|g\rangle\langle g|\}$, $N_e = \mathcal{N} \text{Tr}\{|e\rangle\langle e|\}$ the atomic populations. In this mean-field model the atoms are assumed to identically couple to the mode with an average coupling constant. The effective atom number in the transmission formula of Eq. (1) is then $N = (N_g - N_e)/2$, where the factor $\frac{1}{2}$ accounts for the reduction of the average coupling constant compared to its maximum. With the real atomic level scheme, atoms escape from the two-level space $\{|g\rangle, |e\rangle\}$ from $|g\rangle$ via the state $|i\rangle$. Note that the population in the state $|i\rangle$ is proportional to that in $|e\rangle$; hence the Γ decay term from $|e\rangle$ accounts for the dependence of the loss on the cavity light intensity, without introducing extra variables. On integrating these equations from the appropriate initial conditions, i.e., cavity vacuum, $a = 0$, and all of the atoms in the ground state, $N_g = \mathcal{N}$, $N_e = M = 0$, one can obtain the time evolution of the transmitted intensity signal, $2\kappa|a|^2$, which serves as an order parameter for the phase transition.

This can be seen in Fig. 2, where, focusing on the transition region, the slow crossover from the blocked transmission to the empty cavity phase ($N_g = N_e = 0$) develops into ever faster transition on increasing the laser drive. Three different drive amplitudes are shown, spanning an intensity range of over two orders of magnitude. For the largest power (blue dashed lines), the mean-field solution is matched to the experimental data by using the escape rate, Γ , as the only fitting parameter and the number of atoms is set to $N = 10^4$. For the same value of the escape rate, $\Gamma = 0.93 \times 10^{-3}\gamma$, the slope of the transition around the midpoint exhibits good agreement between measurement and simulation simultaneously for the

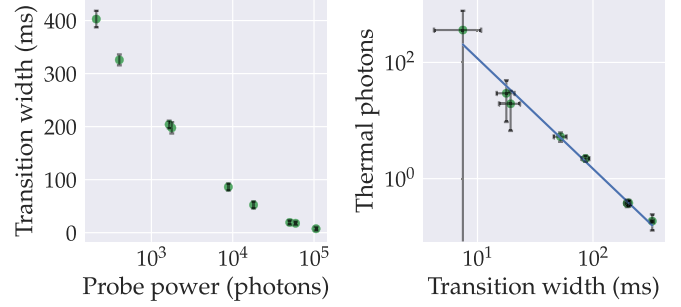


FIG. 3. Left: The width of the transition as a function of the laser drive power, highlighting a finite-size feature of the transition in the transmission blockade breakdown. Right: The scaling of the excess noise in terms of thermal photon number as a function of transition width, where the latter indicates distance from the thermodynamic limit. The power-law fit suggests an exponent of -1.9 ± 0.1 .

other two drive powers, suggesting that the essence of the phase transition dynamics is well captured by Eqs. (3).

IV. FINITE SIZE SCALING AND FLUCTUATIONS

With increasing laser drive power the transition happens more quickly, as plotted in Fig. 3. Here, the transition width was defined as the time taken for the transmitted intensity to rise from 10% to 90% of the resonant empty cavity transmission [cf. the shaded region of the sample trajectory in Fig. 1(e)]. In order to approach the thermodynamic limit, the enhanced drive power should be accompanied by an increasing number of atoms so that the collective dispersive effect counteracts the larger incoming light intensity. On doing such scaling, the transition tends to an instantaneous change. In our experiment the atom number is not varied, however, but the transition width can be operationally used as a measure for how far the system is from the thermodynamic limit.

Our experiment reveals a generic feature of phase transitions beyond the mean-field level, i.e., the emergence of enhanced fluctuations in the course of the transition [40]. The intensity of cavity field fluctuations was extracted from the running variance of the recorded transmission signal with $500 \mu\text{s}$ time resolution. The variance can be connected to the $g^{(2)}$ intensity correlation function of the single-mode field [41–43] which expresses the enhancement of the cavity field fluctuations with respect to the Poissonian statistics. As shown in detail in the Appendix, this excess noise can be expressed in terms of a thermal photon number by using the ansatz for the state of the cavity mode that it is a statistical mixture of coherent states with a Gaussian distribution, $P_{\text{th,disp}}(\alpha) = \frac{1}{\pi n_{\text{th}}} \exp(-|\alpha - \beta|^2/n_{\text{th}})$. This is the P function of a displaced thermal state, with mean field denoted by the complex amplitude β and where the distribution width, n_{th} , can be interpreted as the number of thermally distributed photons. For this mixed state, the intensity correlation function obeys $g^{(2)}(0) = 2 - \frac{|\beta|^4}{(n_{\text{th}} + |\beta|^2)^2}$. This value lies between 1 and 2 for a coherent ($n_{\text{th}} = 0$) and thermal ($\beta = 0$) state, respectively. In the course of the transition, the mean-field amplitude evolves from $\beta = 0$ to $\beta = \eta/\kappa$, as shown in Fig. 1(e). The width of the distribution, n_{th} , also changes during the transition, and

its time-resolved evolution was derived from the measured data, as exemplified in Fig. 1(f). The excess cavity photon fluctuations exhibit a sharp peak in the time evolution, just at the moment where the order parameter transitions from the blockaded phase.

The excess noise with thermal statistics is related to the internal dynamics of the atoms and its description is beyond the scope of our mean-field model (3). In the blockaded regime the transmitted field must be close to a vacuum state. In the transparent phase the transmitted field statistics is expected to retain the Poissonian statistics of the laser source. In between, when the atoms are partially excited, the atomic state can be a statistical mixture of states $|g\rangle$ and $|e\rangle$, which is encoded via the distribution of the probabilities, p_j , in the effective atom number, N , in Eq. (2). This mixture amounts to additional statistical features in the detected field on top of the Poissonian noise.

We show next that the fluctuations generated in the transition increase as a power law as the thermodynamic limit is approached. In Fig. 3, the integrated excess noise in terms of thermal photon number, n_{th} , is plotted as a function of the transition width in a log-log scale together with a power-law fit. This function represents a finite-size scaling. Theoretical confirmation of the measured exponent, -1.9 ± 0.1 , requires more involved modeling. Nevertheless, the good agreement with the fit over two orders of magnitude confirms a characteristic feature of phase transitions, i.e., the power-law divergence of the fluctuations as the thermodynamic limit is approached. We can conclude that the experimentally observed breakdown of the transmission blockade corresponds to a finite-size realization of a genuine phase transition.

V. CONTROL PARAMETER

Finally, let us discuss the control parameter of this phase transition. As it had a fixed value in the presented experiment, the system was only in equilibrium in one of the phases, i.e., in the “bright” phase. In order to vary the control parameter, the system would need an additional, driven, cavity mode at a frequency close to the $(F, m_F) = (1, 1) \leftrightarrow (2, 1)$ transition. This additional laser beam (drive 2) would “repump” the system from the “green” (filled) to the “red” (open) phase in a similar manner to the demonstrated phase transition between the “red” and “green” phases. In the “green” phase, the atoms would be in the state $(F, m_F) = (1, 1)$, with the transmission of the additional laser blockaded because of the same dispersive shift on the respective cavity mode.

This blockade could also break down in a runaway process. If both laser drives were continuously on, there would be a competition between the two directions. Either drive 1 or drive 2 would be transmitted depending on the phase: the atoms in state $(F, m_F) = (1, 1)$ or $(F, m_F) = (2, 2)$ blockading the transmission of the other laser drive, respectively. The photodetector, with a frequency discriminating measurement method (e.g., heterodyning), could then reveal if drive 1 or drive 2 was transmitted, thereby distinguishing the “red” (open) and “green” (filled) phases. In such an extended scheme, the control parameter would be the intensity ratio of the two pump beams, I_1/I_2 . Depending on this ratio, there would be a regime (I_1/I_2 too small or too large) where only

one of the phases is stable. For a given midrange of the ratio there would be a coexistence of phases, i.e., a statistical mixture of the two robust phases. In the time domain one could observe a telegraph signal, a random sequence of transitions between the two phases, as reported in [28] for the case of a photon-blockade breakdown phase transition, and analyzed in [23] in the thermodynamic limit. Within this extended framework, since drive 2 was absent, our experiment represents a single extreme value of the control parameter, $I_1/I_2 = \infty$.

VI. CONCLUSION

Thus, by only considering single transitions at a given value of the control parameter, we could experimentally analyze such important conceptual quantities of phase transitions as thermal fluctuations and finite-size scaling. This analysis refers to criticality in driven-dissipative open systems which is a class of dynamical phase transitions [44]. As a next step, we aim to extend the experiment with a second, laser-driven, cavity mode in order to vary the control parameter and gain access to other regimes of the phase diagram.

ACKNOWLEDGMENTS

This work was supported by the National Research, Development and Innovation Office of Hungary (NKFIH) within the Quantum Technology National Excellence Program (Project No. 2017-1.2.1-NKP-2017-00001) and the Quantum Information National Laboratory of Hungary.

T.W.C. and A.D. contributed equally to this work.

APPENDIX: EXPRESSING THE ENHANCED CAVITY FIELD FLUCTUATIONS IN TERMS OF THERMAL PHOTON NUMBER

Let us assume that the cavity field during the whole time evolution belongs to the class of Gaussian states; that is, the P function is of the general form [41]

$$P_{\text{th,disp}}(\alpha) = \frac{1}{\pi n_{\text{th}}} e^{-\frac{|\alpha-\beta|^2}{n_{\text{th}}}}, \quad (\text{A1})$$

where β gives the displacement amplitude (the “mean field” coherent component), and the width of the distribution, n_{th} , can be interpreted as the number of thermal photons in the state. This state is the *displaced thermal state*. The hypothesis assumes that the source laser field is a coherent state and that the distribution of atoms (both their “random” position and the statistical mixture of the internal state) introduces classical statistics for the cavity field amplitude, β , and Poissonian photon statistics for the coherent state, $|\alpha\rangle$. The transition includes the time evolution of the mean-field amplitude from zero to the stationary amplitude of the resonantly driven empty cavity. Simultaneously, the width of the distribution departs from zero, temporarily, and takes on nonvanishing values in the course of the phase transition.

For a displaced thermal state, it can be straightforwardly calculated that

$$g^{(2)}(0) = \frac{\langle a^\dagger a^\dagger a a \rangle}{\langle a^\dagger a \rangle^2} = 2 - \frac{|\beta|^4}{(n_{\text{th}} + |\beta|^2)^2}, \quad (\text{A2})$$

where it can be seen that $g^{(2)}(0)$ is equal to 2 and 1 for no displacement (a thermal state) and large displacement ($\beta \rightarrow \infty$ or for $n_{\text{th}} \rightarrow 0$), respectively. Thus, the displaced thermal state interpolates the $g^{(2)}(0)$ factors between that of a coherent and a thermal state. For large time differences, τ , the intensity correlation function must obey $g^{(2)}(\tau) \rightarrow 1$. As the field emanating from a cavity is a single-mode field, with homogeneous broadening, the decay of the second-order intensity correlation function must follow an exponential decay,

$$g^{(2)}(\tau) = 1 + c e^{-2\kappa\tau}, \quad (\text{A3})$$

where κ (HWHM) is the Lorentzian linewidth of the cavity mode. The parameter c describes the photon bunching according to Eq. (A2).

Assume a linear relationship between the detector voltage signal and the cavity photon number, $u = \chi \hat{a}^\dagger \hat{a}$. The coefficient χ can be obtained accurately by considering the temporal evolution of the transmission signal statistics. On dividing the raw transmission signal into 500- μs bins, the mean, \bar{u} , and the variance, Δu^2 , could be calculated as discrete functions of time, which were related to the statistical moments of the cavity photon number. The raw signal, however, contained noise components from both the bias-voltage dark current, \tilde{N} , and the amplification (so-called excess noise), F . We therefore assumed that the dark-current noise also had a mean and variance denoted by \bar{N} and ΔN^2 , respectively. The avalanche amplification noise, on the other hand, was represented in the model by taking the coefficient, χ , as a random number, $\tilde{\chi}$, with a mean, $\langle \tilde{\chi} \rangle \equiv \bar{\chi}$, and excess noise factor, $F = \langle \tilde{\chi}^2 \rangle / \bar{\chi}^2 \approx 2$, as this is valid for high avalanche photodiode (APD) gain [45]. Under these conditions, the mean voltage can be simply related to the mean cavity photon number by

$$\bar{u} = \langle \tilde{\chi} \hat{a}^\dagger \hat{a} + \tilde{N} \rangle = \bar{\chi} \langle \hat{a}^\dagger \hat{a} \rangle + \bar{N}, \quad (\text{A4a})$$

where \bar{N} incorporates an arbitrary offset in the voltage measurement. The important dimensional quantity characterizing the whole detection setup is then $\bar{\chi}$, which determines the calibration from measured voltage signal to cavity photon number.

The variance of the voltage fluctuations can be calculated from the Mandel formula [41]. Using the linear relation between the voltage and the photon number, it can be transformed into the form

$$\begin{aligned} \Delta u^2 &= F \bar{\chi} (\bar{u} - \bar{N}) + F (\bar{u} - \bar{N})^2 \\ &\times \left(2 \int_0^T d\tau (1 - \tau) g^{(2)}(t, t + \tau) - 1 \right) + \Delta N^2, \end{aligned} \quad (\text{A4b})$$

where the time resolution T is given by the APD bandwidth (10 MHz in our case, i.e., $T = 100$ ns). The first two moments of the voltage signal are thus related to the input photon signal in an expression that includes the calibration coefficient of the detection setup, $\bar{\chi}$, the excess noise of the APD, F , and

the dark-current noise, ΔN^2 . These quantities can then be calibrated, as follows.

There are two time windows where Eq. (A4b) simplifies considerably: when there are no cavity photons and when $g^{(2)}(t, t + \tau)$ reaches unity. We can first measure the offset and variance of the amplifier noise in the first case, i.e., before the laser shutter is released:

$$\begin{aligned} \bar{N} &= \bar{u} \quad \text{and} \\ \Delta N^2 &= \Delta u^2, \quad \text{for } \langle \hat{a}^\dagger \hat{a} \rangle = 0. \end{aligned}$$

Then, we choose a point where the $g^{(2)}(t, t + \tau)$ function is unity, such as the empty cavity (bright region), where the transmitted light is in a coherent state. For calibration, a better working point is when the drive laser is far away from cavity resonance, and when the drive power is large. Then the classical fluctuations from the cavity lock system are suppressed. In this case the second term on the right-hand side of Eq. (A4b) vanishes, and thus

$$F \bar{\chi} \approx \frac{\Delta u^2 - \Delta N^2}{\bar{u} - \bar{N}}. \quad (\text{A5})$$

As the amplifier offset, \bar{N} , and the dark-current noise, ΔN^2 , are determined from independent measurement data, the calibration coefficient, $\bar{\chi}$, can be obtained from this formula by using the estimated value of the excess noise factor, $F = 2$, valid for high APD gain [45]. In our setup, performing this calibration measurement at $\Delta_C = -2\pi \times 30$ MHz, we obtained the calibration coefficient $\bar{\chi} = 18.44 \mu\text{V}/\text{photons}$. This is in good agreement with the value derived from the specification of the APD and the optical coupling parameters of our setup ($\chi \approx 16 \mu\text{V}/\text{photons}$).

The integral in the Mandel formula, Eq. (A4b), can be evaluated by using the exponential function in Eq. (A3),

$$2 \int_0^1 dx (1 - x) g^{(2)}(0, xT) - 1 = c \left(\frac{1}{\kappa T} + \frac{e^{-2\kappa T} - 1}{2(\kappa T)^2} \right),$$

such that the photon bunching parameter can be deduced from the measurement data as

$$c = \frac{\Delta u^2 - F \bar{\chi} (\bar{u} - \bar{N}) - \Delta N^2}{F (\bar{u} - \bar{N})^2} \left(\frac{1}{\kappa T} + \frac{e^{-2\kappa T} - 1}{2(\kappa T)^2} \right)^{-1}. \quad (\text{A6})$$

The measured c can then be used to express the thermal photon number by inverting Eq. (A2),

$$\frac{n_{\text{th}}}{|\beta|^2} = \frac{1}{\sqrt{1 - c}} - 1, \quad (\text{A7})$$

and using the fact that the displacement corresponds to the mean, i.e., $\bar{u} - \bar{N} = \bar{\chi} |\beta|^2$. The thermal photon number can then be expressed from measured data using

$$n_{\text{th}} = \frac{\bar{u} - \bar{N}}{\bar{\chi}} \left(\frac{1}{\sqrt{1 - c}} - 1 \right). \quad (\text{A8})$$

This value was used to describe the enhanced fluctuations of the cavity field in the paper, where it is referred to as both the thermal noise and, equivalently, the thermal photon number.

- [1] L. A. Lugiato, *II Theory of Optical Bistability* (Elsevier, Amsterdam, 1984), Vol. 21, pp. 69–216.
- [2] P. D. Drummond and D. F. Walls, Quantum theory of optical bistability. II. Atomic fluorescence in a high- Q cavity, *Phys. Rev. A* **23**, 2563 (1981).
- [3] A. T. Rosenberger, L. A. Orozco, and H. J. Kimble, Observation of absorptive bistability with two-level atoms in a ring cavity, *Phys. Rev. A* **28**, 2569 (1983).
- [4] A. T. Rosenberger, L. A. Orozco, H. J. Kimble, and P. D. Drummond, Absorptive optical bistability in two-state atoms, *Phys. Rev. A* **43**, 6284 (1991).
- [5] A. Lambrecht, J. M. Courty, S. Reynaud, and E. Giacobino, Cold atoms: A new medium for quantum optics, *Appl. Phys. B Lasers Opt.* **60**, 129 (1995).
- [6] A. Joshi, A. Brown, H. Wang, and M. Xiao, Controlling optical bistability in a three-level atomic system, *Phys. Rev. A* **67**, 041801(R) (2003).
- [7] Th. Elsässer, B. Nagorny, and A. Hemmerich, Optical bistability and collective behavior of atoms trapped in a high- Q ring cavity, *Phys. Rev. A* **69**, 033403 (2004).
- [8] S. Gupta, K. L. Moore, K. W. Murch, and D. M. Stamper-Kurn, Cavity Nonlinear Optics at Low Photon Numbers from Collective Atomic Motion, *Phys. Rev. Lett.* **99**, 213601 (2007).
- [9] F. Brennecke, S. Ritter, T. Donner, and T. Esslinger, Cavity optomechanics with a Bose-Einstein condensate, *Science* **322**, 235 (2008).
- [10] T. Griesser and H. Ritsch, Nonlinear atom-field dynamics in high- Q cavities: From a BEC to a thermal gas, *Opt. Express* **19**, 11242 (2011).
- [11] H. J. Carmichael, Quantum fluctuations in absorptive bistability without adiabatic elimination, *Phys. Rev. A* **33**, 3262 (1986).
- [12] H. M. Gibbs, S. L. McCall, and T. N. C. Venkatesan, Differential Gain and Bistability Using a Sodium-Filled Fabry-Perot Interferometer, *Phys. Rev. Lett.* **36**, 1135 (1976).
- [13] R. Graham and A. Schenzle, Dispersive optical bistability with fluctuations, *Phys. Rev. A* **23**, 1302 (1981).
- [14] U. Martini, C. Ginzel, and A. Schenzle, Optical bistability and nonclassical photon counting statistics with few atoms, *Opt. Commun.* **102**, 379 (1993).
- [15] J. A. Sauer, K. M. Fortier, M. S. Chang, C. D. Hamley, and M. S. Chapman, Cavity QED with optically transported atoms, *Phys. Rev. A* **69**, 051804(R) (2004).
- [16] G. Rempe, R. J. Thompson, R. J. Brecha, W. D. Lee, and H. J. Kimble, Optical Bistability and Photon Statistics in Cavity Quantum Electrodynamics, *Phys. Rev. Lett.* **67**, 1727 (1991).
- [17] C. M. Savage and H. J. Carmichael, Single atom optical bistability, *IEEE J. Quantum Electron.* **24**, 1495 (1988).
- [18] J. Kerckhoff, M. A. Armen, and H. Mabuchi, Remnants of semiclassical bistability in the few-photon regime of cavity QED, *Opt. Express* **19**, 24468 (2011).
- [19] A. Dombi, A. Vukics, and P. Domokos, Optical bistability in strong-coupling cavity QED with a few atoms, *J. Phys. B: At. Mol. Opt. Phys.* **46**, 224010 (2013).
- [20] M. A. Armen and H. Mabuchi, Low-lying bifurcations in cavity quantum electrodynamics, *Phys. Rev. A* **73**, 063801 (2006).
- [21] H. J. Carmichael, Breakdown of Photon Blockade: A Dissipative Quantum Phase Transition in Zero Dimensions, *Phys. Rev. X* **5**, 031028 (2015).
- [22] A. Dombi, A. Vukics, and P. Domokos, Bistability effect in the extreme strong coupling regime of the Jaynes-Cummings model, *Eur. Phys. J. D* **69**, 60 (2015).
- [23] A. Vukics, A. Dombi, J. M. Fink, and P. Domokos, Finite-size scaling of the photon-blockade breakdown dissipative quantum phase transition, *Quantum* **3**, 150 (2019).
- [24] K. M. Birnbaum, A. Boca, R. Miller, A. D. Boozer, T. E. Northup, and H. J. Kimble, Photon blockade in an optical cavity with one trapped atom, *Nature (London)* **436**, 87 (2005).
- [25] I. Schuster, A. Kubanek, A. Fuhrmanek, T. Puppe, P. W. H. Pinkse, K. Murr, and G. Rempe, Nonlinear spectroscopy of photons bound to one atom, *Nat. Phys.* **4**, 382 (2008).
- [26] T. K. Mavrogordatos, Strong-coupling limit of the driven dissipative light-matter interaction, *Phys. Rev. A* **100**, 033810 (2019).
- [27] X. Gu, A. F. Kockum, A. Miranowicz, Y.-x. Liu, and F. Nori, Microwave photonics with superconducting quantum circuits, *Phys. Rep.* **718-719**, 1 (2017).
- [28] J. M. Fink, A. Dombi, A. Vukics, A. Wallraff, and P. Domokos, Observation of the Photon-Blockade Breakdown Phase Transition, *Phys. Rev. X* **7**, 011012 (2017).
- [29] R. Gutiérrez-Jáuregui and H. J. Carmichael, Dissipative quantum phase transitions of light in a generalized Jaynes-Cummings-Rabi model, *Phys. Rev. A* **98**, 023804 (2018).
- [30] I. Pietikäinen, J. Tuorila, D. S. Golubev, and G. S. Paraoanu, Photon blockade and the quantum-to-classical transition in the driven-dissipative Josephson pendulum coupled to a resonator, *Phys. Rev. A* **99**, 063828 (2019).
- [31] R. Rota, F. Minganti, C. Ciuti, and V. Savona, Quantum Critical Regime in a Quadratically Driven Nonlinear Photonic Lattice, *Phys. Rev. Lett.* **122**, 110405 (2019).
- [32] P. Brookes, G. Tancredi, A. D. Patterson, J. Rahamim, M. Esposito, T. K. Mavrogordatos, P. J. Leek, E. Ginossar, and M. H. Szymanska, Critical slowing down in circuit quantum electrodynamics, *Sci. Adv.* **7**, eabe9492 (2021).
- [33] J. B. Curtis, I. Boettcher, J. T. Young, M. F. Maghrebi, H. Carmichael, A. V. Gorshkov, and M. Foss-Feig, Critical theory for the breakdown of photon blockade, *Phys. Rev. Research* **3**, 023062 (2021).
- [34] F. Reiter, T. L. Nguyen, J. P. Home, and S. F. Yelin, Cooperative Breakdown of the Oscillator Blockade in the Dicke Model, *Phys. Rev. Lett.* **125**, 233602 (2020).
- [35] A. Lambrecht, E. Giacobino, and J. Courty, Optical nonlinear dynamics with cold atoms in a cavity, *Opt. Commun.* **115**, 199 (1995).
- [36] J. C. Bergquist, R. G. Hulet, W. M. Itano, and D. J. Wineland, Observation of Quantum Jumps in a Single Atom, *Phys. Rev. Lett.* **57**, 1699 (1986).
- [37] S. R. K. Rodriguez, W. Casteels, F. Storme, N. Carlon Zambon, I. Sagnes, L. Le Gratiet, E. Galopin, A. Lemaître, A. Amo, C. Ciuti, and J. Bloch, Probing a Dissipative Phase Transition via Dynamical Optical Hysteresis, *Phys. Rev. Lett.* **118**, 247402 (2017).
- [38] Z. Geng, K. J. H. Peters, A. A. P. Trichet, K. Malmir, R. Kolkowski, J. M. Smith, and S. R. K. Rodriguez, Universal Scaling in the Dynamic Hysteresis, and Non-Markovian

- Dynamics, of a Tunable Optical Cavity, *Phys. Rev. Lett.* **124**, 153603 (2020).
- [39] T. Fink, A. Schade, S. Höfling, C. Schneider, and A. Imamoglu, Signatures of a dissipative phase transition in photon correlation measurements, *Nat. Phys.* **14**, 365 (2018).
- [40] B. O. Goes, C. E. Fiore, and G. T. Landi, Quantum features of entropy production in driven-dissipative transitions, *Phys. Rev. Research* **2**, 013136 (2020).
- [41] H. Carmichael, *An Open Systems Approach to Quantum Optics* (Springer-Verlag, Berlin, 1993).
- [42] G. T. Foster, S. L. Mielke, and L. A. Orozco, Intensity correlations of a noise-driven diode laser, *J. Opt. Soc. Am. B* **15**, 2646 (1998).
- [43] E. Overbeck, C. Sinn, I. Flammer, and J. Rička, Silicon avalanche photodiodes as detectors for photon correlation experiments, *Rev. Sci. Instrum.* **69**, 3515 (1998).
- [44] M. Heyl, Dynamical quantum phase transitions: A review, *Rep. Prog. Phys.* **81**, 054001 (2018).
- [45] B. E. A. Saleh and M. C. Teich, *Fundamentals of Photonics* (Wiley, New York, 1991).